# Direct experimental probe of the Ni(II)/Ni(III)/Ni(IV) redox evolution in $LiNi_{0.5}Mn_{1.5}O_4$ electrodes

*Ruimin Qiao[†], Andrew Wray[◊]*, Jung-Hyun Kim[‡], Nicholas P.W. Pieczonka[Δ], Stephen J. Harris[§], Wanli Yang[†]**

[†] Advanced Light Source, Lawrence Berkeley National Laboratory, Berkeley, CA 94720

[◊] Department of Physics, New York University, New York, NY 10003

[‡] Chemical & Materials Systems Laboratory, General Motors Global R&D Center, Warren, MI 48090

[Δ] Optimal CAE Inc, Plymouth, MI 48170

[§] Material Science Division, Lawrence Berkeley National Laboratory, Berkeley, CA 94720

**Corresponding Author**

*wlyang@lbl.gov (W. Y.). *lawray@nyu.edu (A. W.)

KEYWORDS: high voltage spinel, $LiNi_{0.5}Mn_{1.5}O_4$, Ni(III), soft x-ray spectroscopy.

ABSTRACT

$LiNi_{0.5}Mn_{1.5}O_4$ spinel is an appealing cathode material for next generation rechargeable Li-ion batteries due to its high operating voltage of ~4.7 V (vs. $Li/Li^+$). Although it is widely believed that the full range electrochemical cycling involves the redox of Ni(II)/(IV), it has not been experimentally clarified whether Ni(III) exists as the intermediate state, or a double-electron transfer takes place. Here, combined with theoretical calculations, we show unambiguous spectroscopic evidence of the Ni(III) state when the $LiNi_{0.5}Mn_{1.5}O_4$ electrode is half charged. This provides a direct verification of single-electron-transfer reactions in $LiNi_{0.5}Mn_{1.5}O_4$ upon cycling, namely, from Ni(II) to Ni(III), then to Ni(IV). Additionally, by virtue of its surface sensitivity, soft x-ray absorption spectroscopy also reveals the electrochemically inactive $Ni^{2+}$ and $Mn^{2+}$ phases on the electrode surface. Our work provides the long-awaited clarification of the single-electron transfer mechanism in $LiNi_{0.5}Mn_{1.5}O_4$ electrodes. Furthermore, the experimental results serve as a benchmark for further spectroscopic characterizations of Ni-based battery electrodes.

## Introduction

The rapid development of clean sustainable energy technologies over the past decades has stimulated the demand for high-performance electrical energy storage systems such as lithium-ion batteries (LIBs) [1]. Spinel $LiNi_{0.5}Mn_{1.5}O_4$ is an appealing cathode candidate of LIBs for applications in transportation and stationary storage. It is environmentally benign, low-cost, and provides high performance in terms of the energy and power densities [2-5]. The high energy density of $LiNi_{0.5}Mn_{1.5}O_4$ stems from the high operating voltage of 4.7V, which is defined by the $Ni^{2+/4+}$ redox reaction. The electron transfer process associated with this redox reaction is of critical importance for understanding its electrochemical properties. However, it remains elusive whether the $Ni^{2+/4+}$ reaction is a double or single electron transfer process. Although some electrochemical measurements suggest the formation of the intermediate $Ni^{3+}$ state[6-7], direct experimental evidence is missing.

Practically, the commercialization of high-voltage $LiNi_{0.5}Mn_{1.5}O_4$ electrodes encounters several technical challenges[8-12], especially electrolyte degradation at high voltage and transition-metal dissolution. The detailed mechanism of these technical issues has not been fully clarified, but it is believed that the surface activity of the electrode material plays a key role in such detrimental effects. Clarifying the surface reaction is non-trivial, and a multimodal approach is necessary. While the surface characteristics of $LiNi_{0.5}Mn_{1.5}O_4$ electrodes could be studied by transmission electron microscopy (TEM) and x-ray photoelectron spectroscopy (XPS) [7, 13], experimental approaches based on these techniques are still under scrutiny to understand degradation mechanisms associated with the electrode surface and/or interface .

In this work, we have performed high-resolution soft x-ray absorption spectroscopy (sXAS) to study a series of high-quality $LiNi_{0.5}Mn_{1.5}O_4$ electrodes at different electrochemical voltages. sXAS spectra are sensitive to the unoccupied electronic states in the vicinity of the Fermi energy $E_F$. They provide a powerful tool to study the oxidation states, chemical bonds, spin properties and orbital characteristics of the transition-metals involved in battery electrodes [14-15]. Moreover, sXAS is a unique tool that can provide information about both the surface (probe depth of about 10 nm) and the bulk (probe depth of about 100 nm) through the total electron yield (TEY) and total fluorescence yield (TFY), respectively. Our high-resolution sXAS data show clear

transitions between $Ni^{2+}/Ni^{3+}$ and $Ni^{3+}/Ni^{4+}$ redox couples at half-charge, thus providing direct experimental evidence for the single-electron-transfer mechanism in $Li_xNi_{0.5}Mn_{1.5}O_4$ electrodes. In addition, the data reveal that $Ni^{2+}$ and $Mn^{2+}$ phases are formed on the surfaces of the electrodes. The spectral evolution indicates that these di-valent transition-metal phases are electrochemically inactive.

**Experimental Section**

1. Material synthesis, structural and electrochemical characterization

$LiNi_{0.5}Mn_{1.5}O_4$ was synthesized via solid-state reaction. Stoichiometric amounts of $Li_2CO_3$, $NiCO_3$, $MnCO_3$ were mixed using a ball-mill (SPEX 8000D) for 30 min. The mixed precursors were repeatedly ground, pelletized, and heated at the following different temperatures and times in air: 500ºC for 12 h, 650ºC for 12 h, 900ºC for 6 h, and then 700ºC for 2 h. Powder X-ray diffraction (XRD) measurements were carried out with a D8 diffractometer (Bruker) using Cu-Kα1 radiation in Brag-Brentano configuration. Scanning electron microscopy (SEM) images were obtained using Zeiss NVision.

The cathode consisted of 80:10:10 wt% of $LiNi_{0.5}Mn_{1.5}O_4$ spinel, super-P carbon, and polyvinylidene fluoride (PVDF, Kynar HSV900). Lithium foil was used as the anode (half cell). The cathode formulation was mixed with N-methylpyrrolidone (NMP) and coated onto Al foil via the doctor-blade method. A separator (Celgard, PP/PE/PP tri-layer), and 1 M $LiPF_6$ in ethylene carbonate (EC) / ethyl methyl carbonate (EMC) (1/1 vol. ratio) electrolyte were used for preparing coin cells (Hohsen, Al-cladding 2032 model). All coin cells were cycled using a Maccor 4000 battery testing system.

For sXAS experiments, $LiNi_{0.5}Mn_{1.5}O_4$ cathodes were electrochemically cycled in the argon glove box. Afterwards, the cells were disassembled and the cathodes were rinsed with DMC thoroughly to remove any electrolyte and salt residue, and to lock the state-of-charge of the cycled electrodes. The cathode samples were then loaded into the ultra-high vacuum sXAS characterization chamber through a sample transfer kit to avoid any air exposure.[16]

2. Soft x-ray absorption spectroscopy (sXAS) experiments and calculations

sXAS was performed at Beamline 8.0.1 of the Advanced Light Source (ALS) in Lawrence Berkeley National Lab (LBNL). The undulator and spherical grating monochromator supply a linearly polarized photon beam with resolving power up to 6000. The experimental energy resolution is about 0.15eV. Experiments were performed at room temperature and with the linear polarization of the incident beam oriented at 45° to the sample surfaces. The sXAS spectra were collected using both total electron yield (TEY), with a probing depth around 10 nm, and total fluorescence yield (TFY) with a probing depth larger than 100 nm. All the spectra have been normalized to the beam flux measured by the upstream gold mesh.

Calculations were performed for a single impurity Anderson model (SIAM), coupling Ni with a 3 eV wide ligand band that can contain up to one hole. Implementation details for the model are discussed in Ref.[17]. Slater-Condon parameters were renormalized to 80%, 75% and 70% of Hartree-Fock values for nominal $Ni^{2+}$, $Ni^{3+}$ and $Ni^{4+}$ calculations, respectively, and the simulation was thermally populated to 300K. The crystal field was set to 10Dq= 0.5, 2.0, and 2.5, in ascending order for higher valence, and metal-ligand hopping was assigned a similar trend with $V_{eg}$=2, 2.5 and 3 eV. The $t_{2g}$ symmetry hopping parameter was assigned half the amplitude of $e_g$ hopping ($V_{t2g}$=-$V_{eg}$/2). Configuration energies for states with a ligand hole were set to $E(d^{n+1})$-$E(d^n)$=3.5, 0.5, and -2 eV. Core hole configuration energies were set to $E(d^{n+1})$-$E(d^n)$=3.1, -0.9, and -4.4. These parameters result in a high spin state for $Ni^{2+}$, and low spin states for $Ni^{3+}$ and $Ni^{4+}$, and are similar to parameter sets considered in Ref. [17-18].

## Results and Discussion

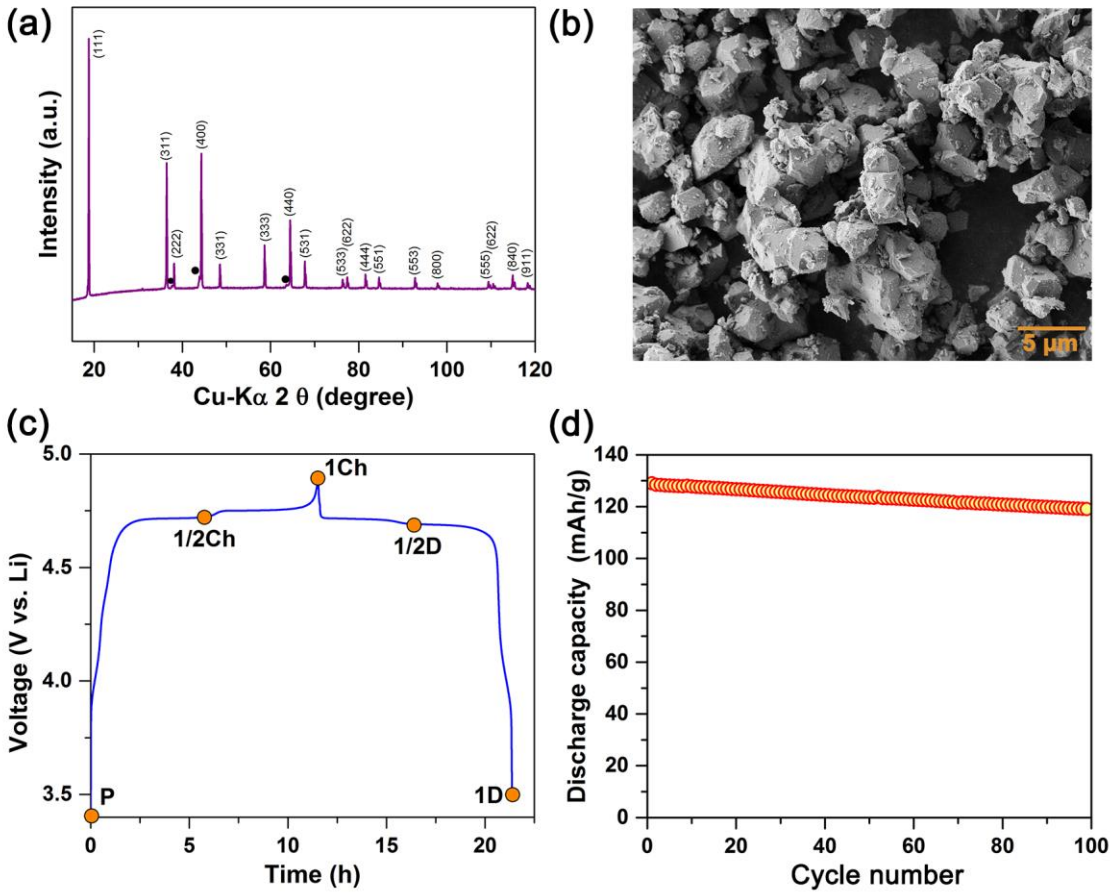


**Figure 1.** (a) XRD pattern of $LiNi_{0.5}Mn_{1.5}O_4$ powder. Extra peaks marked with black dots belong to minor rock-salt (e.g., $Li_{1-x}Ni_xO$) secondary phases. (b) SEM image of $LiNi_{0.5}Mn_{1.5}O_4$ powder. (c) Voltage profiles of $LiNi_{0.5}Mn_{1.5}O_4$ cathode recorded during an initial charge/discharge cycling. The sXAS experiments were performed ex-situ at different states (marked with orange dots): pristine electrode (P), 50 % charge state (1/2Ch), 100 % charge state (1Ch), 50 % discharge state (1/2D), and 100 % discharge state (1D). (d) Capacity retention of $LiNi_{0.5}Mn_{1.5}O_4$/Li battery cell cycled with a C/10-rate at 30°C.

The $LiNi_{0.5}Mn_{1.5}O_4$ spinel powders used in this study have the typical structural and electrochemical characteristics of standard LNMO spectra reported in literature[19]. Figure 1(a) shows the XRD pattern of $LiNi_{0.5}Mn_{1.5}O_4$ powder sample which can be indexed based on cubic symmetry with a space group of *Fd*-3*m*. Minor amounts of secondary phases (~ 4.7 wt %), which

belong to rock-salt structures (e.g., $Li_{1-x}Ni_xO$), also exist in the powder sample[20]. Formation of such rock-salt structures is inevitable during the high temperature (e.g., > 800ºC) synthesis process of $LiNi_{0.5}Mn_{1.5}O_4$ because they are thermodynamically stable at temperatures higher than 700ºC [21-22]. However, these rock-salt phases have been known to be electrochemically inactive in Li-ion battery cells[23]. In Figure 1(b), the SEM image shows that $LiNi_{0.5}Mn_{1.5}O_4$ sample consists of polyhedral particles with approximately 2 – 5 μm diameters.

The cathode prepared by using $LiNi_{0.5}Mn_{1.5}O_4$ spinel powder displays voltage profiles of typical $LiNi_{0.5}Mn_{1.5}O_4$/Li battery cells[19]. Figure 1(c) shows that the $LiNi_{0.5}Mn_{1.5}O_4$ cathode delivers the majority of its capacity through two distinct voltage plateaus at around 4.7 V, which are attributed to $Ni^{2+/4+}$ redox. A small shoulder appears around the 4.1 V region and is associated with $Mn^{3+/4+}$ redox. The formation of Ni-rich rock-salt phases and oxygen deficiencies are responsible for the presence of $Mn^{3+}$ in $LiNi_{0.5}Mn_{1.5}O_4$ [20]. In order to study the major electron transfer process associated with $Ni^{2+/4+}$ redox, comprehensive sXAS experiments were performed at different states (marked with orange dots). The results will be elaborated later. As shown in Fig. 1(d), the $LiNi_{0.5}Mn_{1.5}O_4$/Li cell exhibits initial discharge capacity of ~130 mAh/g, and maintained a good capacity retention: ~ 93% at the 100$^{th}$ cycle (approximately after ~ 3 month testing period) by applying a constant current corresponding to ~ C/10-rate.

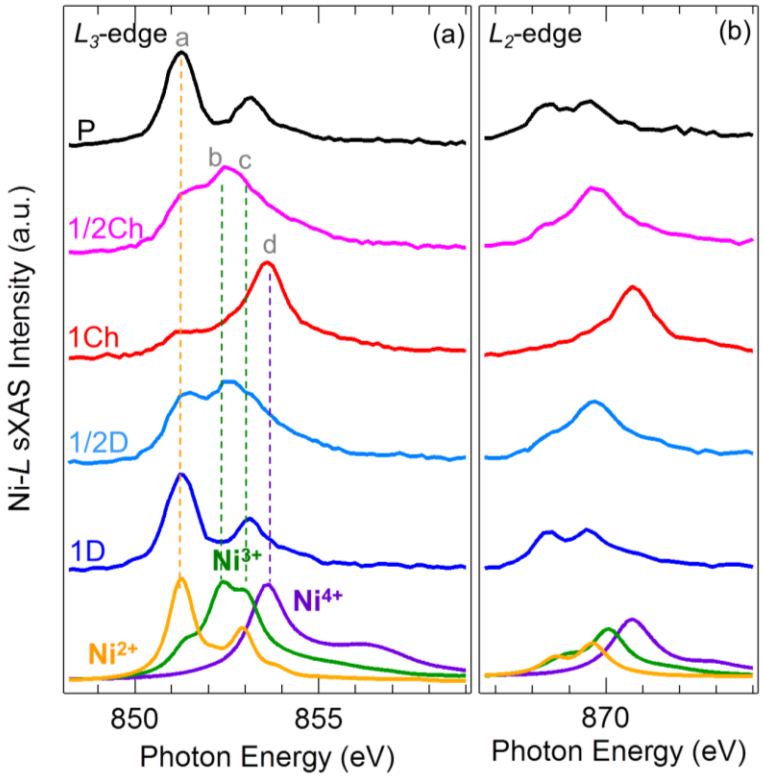


**Figure 2.** Ni $L_3$- (a) and $L_2$-edge (b) TFY sXAS spectra. The experimental spectra were collected on a series of $LiNi_{0.5}Mn_{1.5}O_4$ electrodes that were electrochemically cycled to different states as shown in figure 1(c). The calculated spectra of $Ni^{2+}$, $Ni^{3+}$ and $Ni^{4+}$ were done in an octahedral crystal field.

Soft x-ray absorption spectroscopy studies were carried out on a series of $LiNi_{0.5}Mn_{1.5}O_4$ electrodes that were electrochemically cycled to different states of charge (SOC) as illustrated in figure 1(c). The evolution of the unoccupied valence electron states in $LiNi_{0.5}Mn_{1.5}O_4$, namely, Ni, Mn 3*d* and O 2*p* states, can be directly probed by sXAS spectra through dipole allowed transition metal (TM) 2*p*-3*d* and oxygen 1*s*-2*p* transitions. Therefore, the Ni, Mn *L*- and O *K*-edge sXAS spectra provide abundant information on the electronic states of $LiNi_{0.5}Mn_{1.5}O_4$, and have specific sensitivity to chemical valences of the TM ions, spin and orbital properties, as well as charge transfer between TM ions and ligands. These factors fundamentally regulate the electrochemical properties of the material[14, 16, 24-25].

As shown in figure 2, the reversible evolution of the Ni electronic state in the $LiNi_{0.5}Mn_{1.5}O_4$ electrodes during electrochemical cycling is captured by the Ni *L*-edge TFY (bulk-sensitive) sXAS spectra. The TM *L*-edge sXAS spectra can be divided into two regions, the $L_3$-edge at lower photon energy and the $L_2$-edge at higher energy, due to 2*p* core hole spin-orbital splitting. Both the Ni $L_3$- and the $L_2$-edge sXAS clearly show that the spectral weight shifts towards higher energy during charge and goes back during discharge, which are indicative of increased (decreased) Ni oxidation states during delithiation (lithiation) processes[26]. Moreover, the spectral profile especially on the $L_3$-edge changes dramatically. In general, the $L_2$-edge displays much broader absorption features than the $L_3$-edge due to shorter lifetime of the $2p_{1/2}$ core hole as a consequence of Coster-Kronig Auger decay[27-28]. Therefore, below we will mainly focus on the analysis of the $L_3$-edge absorption profile.

By virtue of the high-resolution bulk-sensitive TFY measurements, Ni absorption features in the electrodes at 50% SOC (1/2Ch and 1/2D) are well distinguished from those at 0% (P and 1D) and 100% SOC (1Ch). Note that the electrodes at 50% SOC have their predominant absorption features (b and c) located at different photon energies from these in 0% (peak a) and 100% SOC (peak d) ones. As a result, the experimental spectra of the 50% SOC electrode samples cannot be reproduced by the combination of the 0% and 100% SOC spectra. This provides direct evidence for the formation of a stable Ni intermediate state in $LiNi_{0.5}Mn_{1.5}O_4$ at 50% SOC. To gain further insight on the evolution of the Ni electronic states, calculations were performed on $Ni^{2+}$, $Ni^{3+}$ and $Ni^{4+}$ in an octahedral crystal field based on a single impurity Anderson model, which improves correspondence relative to a more localized $NiO_6$ cluster. The calculations, which use similar parameter sets to those considered in reference [17-18] result in a high spin state for $Ni^{2+}$, and low spin states for $Ni^{3+}$ and $Ni^{4+}$. The resolved experimental sXAS features on electrodes of 0%, 50% and 100% SOC can be clearly assigned to $Ni^{2+}$, $Ni^{3+}$ and $Ni^{4+}$ [18], respectively. Therefore, the Ni *L*-edge sXAS spectra show unambiguously that $Ni^{3+}$ is the stable intermediate state formed in the electrochemical reaction of the $LiNi_{0.5}Mn_{1.5}O_4$ electrode. In other words, the electrochemical cycling of the $LiNi_{0.5}Mn_{1.5}O_4$ electrode consists of two single electron transfer processes, which involves two redox couples, $Ni^{2+}/Ni^{3+}$ and $Ni^{3+}/Ni^{4+}$ that take place at very close potential[29]. Furthermore, the calculation shows a delocalization of significant hole density (>~0.5 $e^+$/Ni) into nearby oxygen orbitals surrounding $Ni^{3+}$ and $Ni^{4+}$, suggesting the existence of itinerant bands with mixed oxygen/nickel orbital symmetry. These simulated $Ni^{3+}$ ($d7$) and $Ni^{4+}$ ($d6$) states are

stable as a hole does not propagate away from nickel into the ligand bands, and the electron density borrowed from the ligands resides in the mostly vacant $e_g$ orbitals. For example, having a roughly 60% hole density on the oxygens surrounding $Ni^{4+}$ would mean that about 15% of an electron is hybridized into each of the otherwise vacant nickel $e_g$ orbitals. Other than some finer details of core hole shake-up, this scenario may be well described on the great majority of Ni sites by treating $e_g$ states as expanded molecular orbitals. The itinerant property of the electrons in $LiNi_{0.5}Mn_{1.5}O_4$ is associated with the good electronic conductivity of the electrode material.

We would like to point out that although some sXAS results of $LiNi_{0.5}Mn_{1.5}O_4$ have been published previously, typically a broad hump was observed in partially charged $LiNi_{0.5}Mn_{1.5}O_4$ samples. The overall lineshape is consistent with the results here, however, $Ni^{3+}$ cannot be clearly distinguished from $Ni^{2+}$ and $Ni^{4+}$ in these previous works[6, 30]. The bulk-sensitive TFY measurements, combined with the spectra simulation and the high-quality electrode samples, enable us to clearly distinguish the $Ni^{3+}$ phase and to clarify the Ni evolution. Moreover, the surface-sensitive TEY spectra reveal the phases on the surface, in comparison with the bulk phases probed by the TFY mode.

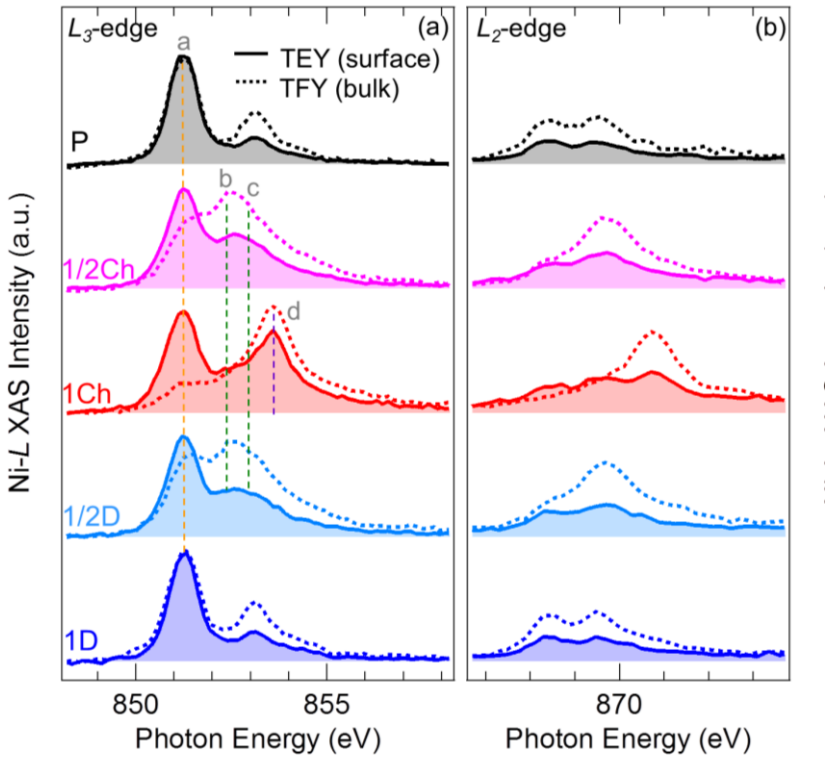

**Figure 3.** Surface-sensitive Ni $L_3$- (a) and $L_2$-edge (b) TEY sXAS spectra (solid lines) are compared with the bulk-sensitive TFY spectra (dash lines) that were also shown in figure 2.

Figure 3 compares the Ni *L*-edge TEY spectra (solid lines) with the TFY (dash lines) that have been discussed above. Compared with TFY, TEY is much more surface-sensitive due to the short escape depth of electrons. The probing depth of TEY is around 10 nm. In general, the TEY spectra of $LiNi_{0.5}Mn_{1.5}O_4$ also evolve following the reversible electrochemical cycling in the same way TFY does. The same absorption features *b* and *c* are observed in the electrodes at 50% SOC (1/2Ch and 1/2D) and *d* at 100% SOC (1Ch), respectively, indicating the electrode surface goes through the same electrochemical reactions as the bulk, i.e., $Ni^{2+}$-$Ni^{3+}$-$Ni^{4+}$. However, unlike TFY, the absorption feature *a* shows the highest intensity among all TEY spectra that were collected at the different SOCs, revealing that a significant amount of nickel on the electrode surface stays at $Ni^{2+}$ in spite of the electrochemical status of the bulk electrode. In contrast, the TFY spectra of the 50% and 100% SOC electrodes contain only minor contributions of $Ni^{2+}$ signal (peak *a*), which is mainly from the electrode surface (Fig. 3).

The observation of strong TEY signals of $Ni^{2+}$ in all the samples with different SOC indicates the existence of a $Ni^{2+}$ surface layer that is electrochemically inactive. Recently, surface rearrangement with inactive $Ni^{2+}$ phase has been reported[31-32]. Moreover, reactions between the $LiNi_{0.5}Mn_{1.5}O_4$ electrodes and electrolytes lead to the deposition of a decomposition product of the electrolyte and the reduction of transition metals in the active materials[30]. Additionally, transition metal dissolution phenomena from the surfaces of $LiNi_{0.5}Mn_{1.5}O_4$ cathodes result in the production of metal fluorides (e.g., $NiF_2$, $MnF_2$, and LiF) and $Ni^{2+}/Mn^{2+/3+}$ β-diketonate coordination complexes[7], which will be responsible for the $Ni^{2+}$ signal from the TEY spectra. Although it has been generally believed that these surface species cannot perfectly passivate the CEI, we recently demonstrated that there is a limited role from the surface species on cycled $LiNi_{0.5}Mn_{1.5}O_4$ cathodes to serve as a passivation layer[13, 33]. However, it should be remembered that the stability and effectiveness of such surface species as a passivation layer is not satisfactory and is still questionable based on the continuous electrolyte degradation occurring in $LiNi_{0.5}Mn_{1.5}O_4$/graphite full cells[33].

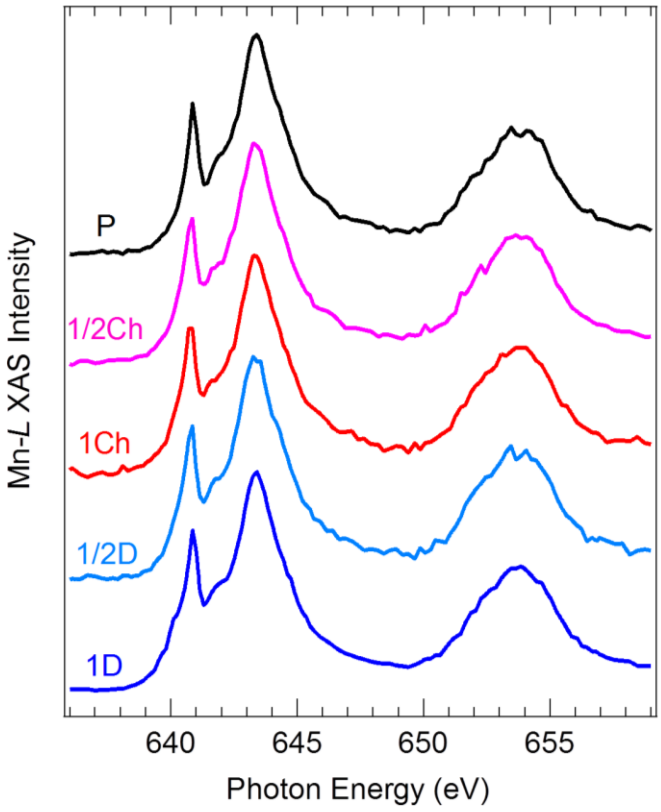


**Figure 4.** Mn *L*-edge sXAS spectra (TEY) of a series of $LiNi_{0.5}Mn_{1.5}O_4$ electrodes at different SOCs.

Similar to Ni, the Mn *L*-edge sXAS spectra are very sensitive to the Mn oxidation states. Manganese compounds with different Mn valences display dramatically different absorption profiles[16]. As shown in figure 3, the Mn *L*-edge sXAS spectra (TEY) collected on a series of $LiNi_{0.5}Mn_{1.5}O_4$ electrodes at different SOCs exhibit nearly the same shape. The spectra consist of Mn $L_3$-edge (639 eV – 647 eV) and $L_2$-edge (650 eV – 657 eV) absorption features. The peak positions and the overall lineshape resemble the $Mn^{4+}$ system in a cubic ligand field [16, 30]. The nearly unchanged Mn-*L* sXAS spectra confirm that $Mn^{4+}$ is electrochemically inactive in the $LiNi_{0.5}Mn_{1.5}O_4$ electrode. Note the faint growth of leading edge absorption intensity around 640 eV, especially in sample 1D, which stems from the formation of manganese compounds with $Mn^{2+}/Mn^{3+}$ on the electrode surface. This is again related to the $Mn^{2+}$ dissolution issue at the surface of $LiNi_{0.5}Mn_{1.5}O_4$ electrodes, as discussed above [9].

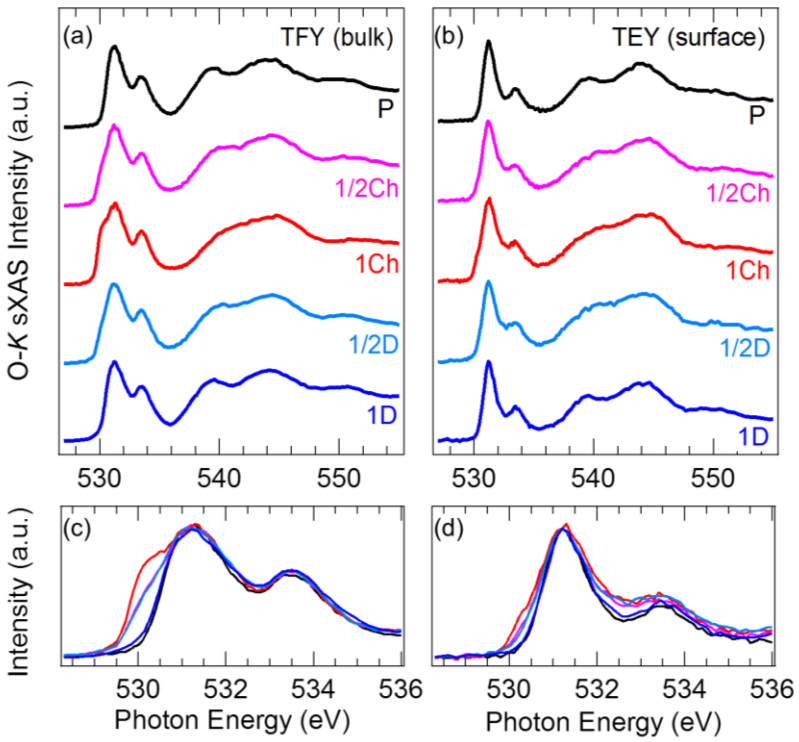


**Figure 5.** O *K*-edge sXAS spectra of a series of $LiNi_{0.5}Mn_{1.5}O_4$ electrodes at different SOCs. (a) and (c), bulk-sensitive TFY, (b) and (d) surface-sensitive TEY.

Figure 5 shows the O *K*-edge sXAS spectra collected on a series of $LiNi_{0.5}Mn_{1.5}O_4$ electrodes at different SOCs. The O *K*-edge sXAS spectra originate from an oxygen 1*s*-2*p* dipole transition. The features of the spectra (Fig. 5a and 5b)are roughly divided into two regions, i.e., the pre-edge region (529 – 536 eV) with sharp peaks, which originate from the hybridization states between O-2*p* and localized TM-3*d* orbitals, and the broad peak region (above 536 eV), which is related to the itinerary O-2*p* and TM-4*s,p* hybridization[34]. Both regions evolve systematically with the SOCs of the electrodes. The pre-edge absorption region in O *K*-edge sXAS, which reflects the transition metal Ni and Mn 3*d* states, is focused in figure 5 (c) and (d). The $LiNi_{0.5}Mn_{1.5}O_4$ electrodes with 0% SOC (P and 1D) display two peaks related to $Ni^{2+}$ ($3d^8$) and $Mn^{4+}$ ($3d^3$). When the electrodes are charged and electrons are removed from the system through the delithiation process. Compared with the pristine $Ni^{2+}$ ($3d^8$) state, the newly emptied Ni 3*d* states of the $Ni^{3+}$ ($3d^7$) and $Ni^{4+}$ ($3d^6$) (Fig. 2) manifest themselves in the O-*K* spectra through the hybridization feature at the lower energy at 530eV (Fig. 5c). The contrast between the O-*K* surface-sensitive TEY signal (Fig. 5b, d) and bulk-sensitive TFY signal (Fig.5a, c) resembles

that of the Ni-*L* edges (Fig. 3). The spectral evolution of the TEY (Fig. 5d) data is much weaker than that of the TFY (Fig.5c), which is consistent with the aforementioned electrochemically inactive $Ni^{2+}$ phase on the electrode surface.

The sXAS features above 536eV become broader at the delithiation state (1Ch), and get sharpened when the material is lithiated (1D). The observed spectral broadening could stem from more itinerant electrons[35-36] and/or structural distortion[37] of the electrode material under delithiated states. We note that a direct measurement of the electronic conductivity of a cycled $Li_{1-x}Ni_{0.5}Mn_{1.5}O_4$ material is non-trivial due to the existence of the conductive carbon. A recent work on $Li_{1-x}Ni_{0.5}Mn_{1.5}O_4$ thin films indicates the decrease of impedance of partially delithiated $Li_{1-x}Ni_{0.5}Mn_{1.5}O_4$ samples[38]. In the meantime, the lattice of electrode materials often gets distorted and disordered during a delithiation process, which may also contribute to the spectral broadening.

**Conclusions**

In conclusion, we performed comprehensive soft x-ray absorption spectroscopy studies, including Ni, Mn *L*-edge and O *K*-edge on $LiNi_{0.5}Mn_{1.5}O_4$ electrodes at different electrochemical states. The Ni *L*-edge data show three distinct lineshapes at the discharged, half-charged, and charged states. The lineshapes correspond to dominant $Ni^{2+}$, $Ni^{3+}$ and $Ni^{4+}$ phases at the different SOCs, as interpreted by the multiplet calculations. The combined spectroscopic and theoretical data provide direct evidence for single-electron-transfer reactions in the $LiNi_{0.5}Mn_{1.5}O_4$ electrode upon cycling, namely, $Ni^{2+}/Ni^{3+}$ and $Ni^{3+}/Ni^{4+}$. Moreover, an electrochemically inactive $Ni^{2+}$ and $Mn^{2+}$ phase is observed on the electrode surface, in contrast to the bulk phases that follow the redox reaction upon electrochemical cycling. With regard to the experimental technique, this work is another demonstration of the power of soft x-ray spectroscopy for clarifying the electronic and chemical state evolution of 3*d* transition-metal based battery electrodes.

AUTHOR INFORMATION

ACKNOWLEDGMENT

The Advanced Light Source is supported by the Director, Office of Science, Office of Basic Energy Sciences, of the U.S. Department of Energy under Contract No. DE-AC02-05CH11231. Ruimin Qiao is supported by the LDRD program at the Lawrence Berkeley National Laboratory. This work was supported partially by the MRSEC Program of the National Science Foundation under Award Number DMR-1420073. Steve Harris is supported by the Assistant Secretary for Energy Efficiency and Renewable Energy, Office of Vehicle Technologies of the U.S. Department of Energy under Contract No. DE-AC02-05CH11231, under the Advanced Battery Material Research (BMR) Program.

REFERENCES

1. Armand, M.; Tarascon, J. M. Building Better Batteries. *Nature* **2008,** *451*, 652-657.
2. Zhong, Q.; Bonakdarpour, A.; Zhang, M.; Gao, Y.; Dahn, J. R. Synthesis and Electrochemistry of $LiNi_xMn_{2-x}O_4$. *J. Electrochem. Soc.* **1997,** *144*, 205-213.
3. Santhanam, R.; Rambabu, B. Research Progress in High Voltage Spinel $LiNi_{0.5}Mn_{1.5}O_4$ Material. *J. Power Sources* **2010,** *195*, 5442-5451.
4. Hassoun, J.; Lee, K.-S.; Sun, Y.-K.; Scrosati, B. An Advanced Lithium Ion Battery Based on High Performance Electrode Materials. *J. Am. Chem. Soc.* **2011,** *133*, 3139-3143.
5. Liu, D.; Zhu, W.; Trottier, J.; Gagnon, C.; Barray, F.; Guerfi, A.; Mauger, A.; Groult, H.; Julien, C. M.; Goodenough, J. B., et al. Spinel Materials for High-Voltage Cathodes in Li-ion Batteries. *RSC Advances* **2014,** *4*, 154-167.
6. Okumura, T.; Shikano, M.; Kobayashi, H. Contribution of oxygen partial density of state on lithium intercalation/de-intercalation process in $Li_xNi_{0.5}Mn_{1.5}O_4$ spinel oxides. *J. Power Sources* **2013,** *244*, 544-547.
7. Aurbach, D.; Markovsky, B.; Talyossef, Y.; Salitra, G.; Kim, H.-J.; Choi, S. Studies of Cycling Behavior, Ageing, and Interfacial Reactions of $LiNi_{0.5}Mn_{1.5}O_4$ and Carbon Electrodes for Lithium-Ion 5-V Cells. *J. Power Sources* **2006,** *162*, 780-789.
8. von Cresce, A.; Xu, K. Electrolyte Additive in Support of 5V Li Ion Chemistry. *J. Electrochem. Soc.* **2011,** *158*, A337-A342.
9. Pieczonka, N. P. W.; Liu, Z.; Lu, P.; Olson, K. L.; Moote, J.; Powell, B. R.; Kim, J.-H. Understanding Transition-Metal Dissolution Behavior in $LiNi_{0.5}Mn_{1.5}O_4$ High-Voltage Spinel for Lithium Ion Batteries. *J. Phys. Chem. C* **2013,** *117*, 15947-15957.

10. Norberg, N. S.; Lux, S. F.; Kostecki, R. Interfacial Side-Reactions at a $LiNi_{0.5}Mn_{1.5}O_4$ Electrode in Organic Carbonate-Based Electrolytes. *Electrochem. Commun.* **2013,** *34*, 29-32.
11. Delacourt, C.; Kwong, A.; Liu, X.; Qiao, R.; Yang, W. L.; Lu, P.; Harris, S. J.; Srinivasan, V. Effect of Manganese Contamination on the Solid-Electrolyte-Interphase Properties in Li-Ion Batteries. *J. Electrochem. Soc.* **2013,** *160*, A1099-A1107.
12. Komaba, S.; Kumagai, N.; Kataoka, Y. Influence of Manganese(II), Cobalt(II), and Nickel(II) Additives in Electrolyte on Performance of Graphite Anode for Lithium-ion Batteries. *Electrochim. Acta* **2002,** *47*, 1229-1239.
13. Kim, J.-H.; Pieczonka, N. P. W.; Yang, L. Challenges and Approaches for High-Voltage Spinel Lithium-Ion Batteries. *ChemPhysChem* **2014,** *15*, 1940-1954.
14. Yang, W.; Liu, X.; Qiao, R.; Olalde-Velasco, P.; Spear, J. D.; Roseguo, L.; Pepper, J. X.; Chuang, Y.-d.; Denlinger, J. D.; Hussain, Z. Key Electronic States in Lithium Battery Materials Probed by Soft X-ray Spectroscopy. *J. Electron Spectrosc. Relat. Phenom.* **2013,** *190*, 64-74.
15. Qiao, R. M.; Lucas, I. T.; Karim, A.; Syzdek, J.; Liu, X. S.; Chen, W.; Persson, K.; Kostecki, R.; Yang, W. L. Distinct Solid-Electrolyte-Interphases on Sn (100) and (001) Electrodes Studied by Soft X-Ray Spectroscopy. *Advanced Materials Interfaces* **2014,** *1*.
16. Qiao, R.; Chin, T.; Harris, S. J.; Yan, S.; Yang, W. Spectroscopic Fingerprints of Valence and Spin States in Manganese Oxides and Fluorides. *Curr. Appl. Phys.* **2013,** *13*, 544-548.
17. Matsubara, M.; Uozumi, T.; Kotani, A.; Claude Parlebas, J. Charge Transfer Excitation in Resonant X-ray Emission Spectroscopy of NiO. *J. Phys. Soc. Jpn.* **2005,** *74*, 2052-2060.
18. Piamonteze, C.; de Groot, F. M. F.; Tolentino, H. C. N.; Ramos, A. Y.; Massa, N. E.; Alonso, J. A.; Martínez-Lope, M. J. Spin-Orbit-Induced Mixed-Spin Ground State in $RNiO_3$ Perovskites Probed by X-ray Absorption Spectroscopy: Insight into the Metal-to-Insulator Transition. *Phys. Rev. B* **2005,** *71*, 020406.
19. Manthiram, A.; Chemelewski, K.; Lee, E.-S. A Perspective on the High-Voltage $LiMn_{1.5}Ni_{0.5}O_4$ Spinel Cathode for Lithium-Ion Batteries. *Energy Environ. Sci.* **2014,** *7*, 1339-1350.
20. Kim, J.-H.; Huq, A.; Chi, M.; Pieczonka, N. P. W.; Lee, E.; Bridges, C. A.; Tessema, M. M.; Manthiram, A.; Persson, K. A.; Powell, B. R. Integrated Nano-Domains of Disordered and Ordered Spinel Phases in $LiNi_{0.5}Mn_{1.5}O_4$ for Li-Ion Batteries. *Chem. Mater.* **2014,** *26*, 4377-4386.
21. Kunduraci, M.; Amatucci, G. G. Effect of Oxygen Non-Stoichiometry and Temperature on Cation Ordering in $LiMn_{2-x}Ni_xO_4$ ($0.5 \geq x \geq 0.36$) Spinels. *J. Power Sources* **2007,** *165*, 359-367.
22. Song, J.; Shin, D. W.; Lu, Y.; Amos, C. D.; Manthiram, A.; Goodenough, J. B. Role of Oxygen Vacancies on the Performance of $Li[Ni_{0.5-x}Mn_{1.5+x}]O_4$ (x = 0, 0.05, and 0.08) Spinel Cathodes for Lithium-Ion Batteries. *Chem. Mater.* **2012,** *24*, 3101-3109.
23. Zheng, J.; Xiao, J.; Yu, X.; Kovarik, L.; Gu, M.; Omenya, F.; Chen, X.; Yang, X.-Q.; Liu, J.; Graff, G. L., et al. Enhanced $Li^+$ ion transport in $LiNi_{0.5}Mn_{1.5}O_4$ through Control of Site Disorder. *Phys. Chem. Chem. Phys.* **2012,** *14*, 13515-13521.
24. Liu, X.; Liu, J.; Qiao, R.; Yu, Y.; Li, H.; Suo, L.; Hu, Y.-s.; Chuang, Y.-D.; Shu, G.; Chou, F., et al. Phase Transformation and Lithiation Effect on Electronic Structure of $Li_xFePO_4$: an In-Depth Study by Soft X-Ray and Simulations. *J. Am. Chem. Soc.* **2012,** *134*, 13708-13715.
25. Wang, L.; Song, J.; Qiao, R.; Wray, L. A.; Hossain, M. A.; Chuang, Y. D.; Yang, W.; Lu, Y.; Evans, D.; Lee, J. J., et al. Rhombohedral Prussian White as Cathode for Rechargeable Sodium-Ion Batteries. *J. Am. Chem. Soc.* **2015,** *137*, 2548-54.

26. Wang, H.; Ge, P.; Riordan, C. G.; Brooker, S.; Woomer, C. G.; Collins, T.; Melendres, C. A.; Graudejus, O.; Bartlett, N.; Cramer, S. P. Integrated X-ray L Absorption Spectra. Counting Holes in Ni Complexes. *J. Phys. Chem. B* **1998,** *102*, 8343-8346.
27. Zaanen, J.; Sawatzky, G. A. Strong Interference Between Decay Channels and Valence-Electron Rearrangements in Core-Hole Spectroscopy. *Phys. Rev. B* **1986,** *33*, 8074-8083.
28. de Groot, F. M. F.; Fuggle, J. C.; Thole, B. T.; Sawatzky, G. A. 2*p* X-Ray Absorption of 3*d* Transition-Metal Compounds: An Atomic Multiplet Description Including the Crystal Field. *Phys. Rev. B* **1990,** *42*, 5459-5468.
29. Evans, D. H. One-Electron and Two-Electron Transfers in Electrochemistry and Homogeneous Solution Reactions. *Chem. Rev.* **2008,** *108*, 2113-2144.
30. Qiao, R.; Wang, Y.; Olalde-Velasco, P.; Li, H.; Hu, Y.-S.; Yang, W. Direct Evidence of Gradient Mn(II) Evolution at Charged States in $LiNi_{0.5}Mn_{1.5}O_4$ Electrodes with Capacity Fading. *J. Power Sources* **2015,** *273*, 1120-1126.
31. Lin, F.; Markus, I. M.; Nordlund, D.; Weng, T.-C.; Asta, M. D.; Xin, H. L.; Doeff, M. M. Surface Reconstruction and Chemical Evolution of Stoichiometric Layered Cathode Materials for Lithium-Ion Batteries. *Nat. Commun.* **2014,** *5*.
32. Lin, M.; Ben, L.; Sun, Y.; Wang, H.; Yang, Z.; Gu, L.; Yu, X.; Yang, X.-Q.; Zhao, H.; Yu, R., et al. Insight into the Atomic Structure of High-Voltage Spinel LiNi0.5Mn1.5O4 Cathode Material in the First Cycle. *Chem. Mater.* **2015,** *27*, 292-303.
33. Kim, J.-H.; Pieczonka, N. P. W.; Lu, P.; Liu, Z.; Qiao, R.; Yang, W.; Tessema, M. M.; Sun, Y.-K.; Powell, B. R. In Situ Formation of a Cathode–Electrolyte Interface with Enhanced Stability by Titanium Substitution for High Voltage Spinel Lithium-Ion Batteries. *Advanced Materials Interfaces* **2015,** *2*, 1500109-1500121.
34. de Groot, F. M. F.; Grioni, M.; Fuggle, J. C.; Ghijsen, J.; Sawatzky, G. A.; Petersen, H. Oxygen 1*s* X-Ray Absorption Edges of Transition-Metal Oxides. *Phys. Rev. B* **1989,** *40*, 5715-5723.
35. de Groot, F.; Kotani, A., *Core Level Spectroscopy of Solids*. CRC Press Taylor & Francis Group: Boca Raton, FL, USA, 2008.
36. Yang, W. L.; Sorini, A. P.; Chen, C. C.; Moritz, B.; Lee, W. S.; Vernay, F.; Olalde-Velasco, P.; Denlinger, J. D.; Delley, B.; Chu, J. H., et al. Evidence for weak electronic correlations in iron pnictides. *Phys. Rev. B* **2009,** *80*, 014508.
37. de Groot, F. M. F.; Faber, J.; Michiels, J. J. M.; Czyżyk, M. T.; Abbate, M.; Fuggle, J. C. Oxygen 1 \textit{s} x-ray absorption of tetravalent titanium oxides: A comparison with single-particle calculations. *Phys. Rev. B* **1993,** *48*, 2074-2080.
38. Gellert, M.; Gries, K. I.; Zakel, J.; Kranz, S.; Bradler, S.; Hornberger, E.; Müller, S.; Yada, C.; Rosciano, F.; Volz, K., et al. Charge Transfer across the Interface between LiNi0.5Mn1.5O4 High-Voltage Cathode Films and Solid Electrolyte Films. *J. Electrochem. Soc.* **2015,** *162*, A754-A759.

TOC: